Tokamak-like confinement at a high beta and low toroidal field in the MST reversed field pinch*

J.S. Sarff[1], A.F. Almagri[1], J.K. Anderson[1], T.M. Biewer[1], A.P. Blair[1], M. Cengher[1], B.E. Chapman[1], P.K. Chattopadhyay[1], D. Craig[1], D.J. Den Hartog[1], F. Ebrahimi[1], G. Fiksel[1], C.B. Forest[1], J.A. Goetz[1], D. Holly[1], B. Hudson[1], T.W. Lovell[1], K.J. McCollam[1], P.D. Nonn[1], R. O'Connell[1], S.P. Oliva[1], S.C. Prager[1], J.C. Reardon[1], M.A. Thomas[1], M.D. Wyman[1], D.L. Brower[2], W.X. Ding[2], S.D. Terry[2], M.D. Carter[3], V.I. Davydenko[4], A.A. Ivanov[4], R.W. Harvey[5], R.I. Pinsker[6] and C. Xiao[7]

[1] University of Wisconsin-Madison, Madison, WI, USA
[2] Electrical Engineering Department, University of California, Los Angeles, CA, USA
[3] Oak Ridge National Laboratory, Oak Ridge, TN, USA
[4] Budker Institute of Nuclear Physics, Novosibirsk, Russia
[5] CompX, Del Mar, CA, USA
[6] General Atomic, LaJolla, CA, USA
[7] University of Saskatchewan, Saskatoon, Saskatchewan, Canada

E-mail: jssarff@wisc.edu

Abstract
Energy confinement comparable with tokamak quality is achieved in the Madison Symmetric Torus (MST) reversed field pinch (RFP) at a high beta and low toroidal magnetic field. Magnetic fluctuations normally present in the RFP are reduced via parallel current drive in the outer region of the plasma. In response, the electron temperature nearly triples and beta doubles. The confinement time increases ten-fold (to ∼10 ms), which is comparable with L- and H-mode scaling values for a tokamak with the same plasma current, density, heating power, size and shape. Runaway electron confinement is evidenced by a 100-fold increase in hard x-ray bremsstrahlung. Fokker–Planck modelling of the x-ray energy spectrum reveals that the high energy electron diffusion is independent of the parallel velocity, uncharacteristic of magnetic transport and more like that for electrostatic turbulence. The high core electron temperature correlates strongly with a broadband reduction of resonant modes at mid-radius where the stochasticity is normally most intense. To extend profile control and add auxiliary heating, rf current drive and neutral beam heating are in development. Low power lower-hybrid and electron Bernstein wave injection experiments are underway. Dc current sustainment via ac helicity injection (sinusoidal inductive loop voltages) is also being tested. Low power neutral beam injection shows that fast ions are well-confined, even in the presence of relatively large magnetic fluctuations.

PACS numbers: 52.55.Dy, 52.55.Hc, 52.55.Fa, 52.35.Ra

1. Introduction

The reversed field pinch (RFP) configuration represents toroidal fusion plasma confinement in the limit where the magnetic field is small and strongly sheared. In particular, the toroidal magnetic field applied at the plasma boundary is typically ∼100 times smaller than for a tokamak with the same plasma current. The potential benefits of a fusion reactor based on the RFP include high beta, high power density, small forces on normal-conducting magnet coils, simple assembly and the possibility of Ohmic ignition [1]. The 'engineering beta' is

---

* Presented at the 19th IAEA Fusion Energy Conference with the title *Overview of Improved Confinement and Plasma Control in the MST Reversed Field Pinch.*

particularly large since the field at the magnet coils is small. Demonstration of fusion-relevant plasma confinement in a relatively weak magnetic field has been the principal challenge for RFP research. In this paper we describe the confinement of $T_e > 1$ keV plasmas with an electron heat transport conductivity $\chi_e \sim 5$–10 m^2 s^{-1} in the Madison Symmetric Torus (MST) RFP, comparable with the heat transport rate in a tokamak plasma with a magnetic field strength ten times larger at the plasma surface.

Large radial transport from parallel streaming in a stochastic magnetic field must be avoided in any fusion plasma. Toroidal configurations with strong external magnetization tend not to suffer this problem. This is not the case for a standard RFP plasma formed by steady toroidal induction, which is unstable to resistive MHD tearing and relies on a fluctuation-induced emf (e.g. the MHD dynamo $\langle \tilde{V} \times \tilde{B} \rangle$) to sustain essential poloidal current flowing in the outer region of the plasma. The standard RFP fusion development path depends on a large reduction of the dynamo's constituent tearing fluctuations as the plasma's electrical resistivity decreases. The scaling of these fluctuations is subject to resistive MHD physics and is not very favourable to date [2, 3]. It has been suggested that the dynamo emf might be obtained with a single, large instability, avoiding multiple island formation and the widespread magnetic stochasticity that normally occurs. Such a 'single-helicity' dynamo has been observed in MHD computation [4, 5], but not yet in experiments. However, 'quasi-single-helicity' conditions in which one mode spontaneously grows larger are observed, thought to be a partial transition to single-helicity [6].

A different RFP fusion development path based on external current drive to maintain a stable current profile has emerged in recent years. This requires the addition of poloidal current drive for improved plasma stability or, equivalently, for the replacement of the dynamo emf present in standard RFP sustainment. The current profile and toroidal field reversal are maintained directly, rather than relying on the dynamo to redistribute current within the plasma. The anticipated reduction in magnetic stochasticity brought about by current profile control is illustrated in figure 1. The field line puncture plot shown in figure 1(a) is for a standard RFP plasma in which several large tearing modes cause the magnetic field

to become stochastic over most of the plasma volume. In contrast, the puncture plot in figure 1(b) shows greatly reduced magnetic stochasticity when auxiliary current drive is added at $r/a \sim 0.8$, thereby improving the stability of the parallel current profile. These puncture plots were generated from three-dimensional (cylindrical) resistive MHD simulations that model the non-linear dynamical evolution of MHD tearing in the RFP, with and without auxiliary current drive. The optimum auxiliary current drive is localized to the outer region, $0.7 < r/a < 0.9$, of the plasma [7].

The improvement in energy confinement associated with the transition from the stochastic magnetic field represented in figure 1(a) to the more ordered magnetic field in figure 1(b) is the focus of this paper. Although precise current profile control is not yet available for RFP experiments, time-dependent inductive electric field programming has proven to be a simple and effective means to reduce magnetic fluctuations. A programmed ramp of the toroidal field winding current is used to generate poloidal induction targeted to the outer region of the plasma, a technique referred to as pulsed poloidal (or parallel) current drive (PPCD) [8–11]. Current drive based on rf techniques is in development for MST, briefly described in section 5. When PPCD programming is applied to MST plasmas, energy and particle confinement greatly improve. The core electron temperature increases nearly three-fold while the Ohmic input power decreases, unambiguous evidence of reduced electron heat transport. The substantial temperature gradient, usually confined to a narrow edge region in standard RFP plasmas, extends into the core during PPCD. Fast electrons become confined, evidenced by a $\sim$100-fold increase in hard x-ray bremsstrahlung emission. Fokker–Planck modelling reveals that the diffusion of these electrons does not depend on their parallel velocity and is no longer characteristically stochastic magnetic in origin. The global energy confinement time increases ten-fold to a value comparable with L- and H-mode expectations for a tokamak of the same current, density, size and shape.

In the following sections we describe these confinement-related results in more detail, along with progress in quantitative understanding of energy transport in a stochastic magnetic field. We also briefly describe progress in developing plasma control tools for MST using rf current drive and heating, neutral beam heating and oscillating field current drive (OFCD).

2. Tokamak-like energy confinement at a high beta in MST

The MST is a circular cross-section torus with dimensions $R = 1.5$ m and $a = 0.5$ m (large for RFP experiments) and toroidal current $I_\phi \leqslant 0.5$ MA [12]. The standard fuelling is deuterium. The inductive current drive programming for PPCD is illustrated in figure 2. The toroidal, E_ϕ, and poloidal, E_θ, electric fields (from loop voltages) applied at the plasma surface are shown in figure 2(a). The essential ingredient for PPCD is $E_\theta > 0$, accomplished with circuitry that ramps the toroidal field winding current in time. As a byproduct, the edge toroidal field, $B_\phi(a)$, and safety factor, $q = rB_\phi/RB_\theta$, become more negative during this time. The parallel inductive electric field, $E_\parallel = (E_\phi B_\phi + E_\theta B_\theta)/B$, is shown in figure 2(b)
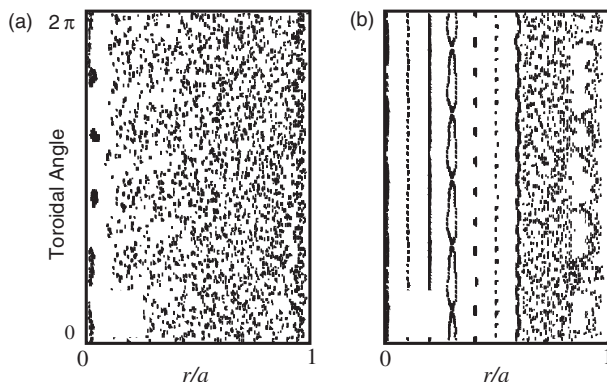

Figure 1. Field line puncture plots in the axial (toroidal) plane for (a) the standard RFP formed by steady toroidal induction and (b) current profile-controlled RFP with auxiliary current drive at $r/a \sim 0.8$ (from [26]).
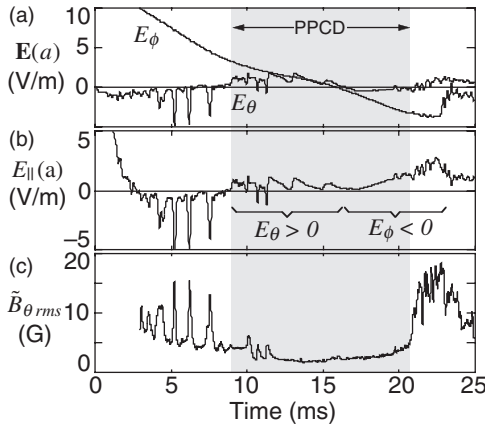
Figure 2. (*a*) Toroidal and poloidal inductive electric field, (*b*) parallel electric field and (*c*) rms poloidal magnetic fluctuation amplitude at $r = a$. The sawtooth-like E_θ waveform results from a five-stage capacitor bank network used for PPCD. The B_θ fluctuation results primarily from $m = 1$ modes resonant in the core.

to emphasize the desired goal, $E_\parallel > 0$, for direct sustainment of parallel current in the outer region of the plasma. The typical reduction in the rms magnetic fluctuation amplitude measured at the plasma surface is shown in figure 2(*c*). The dominant fluctuations are from resistive MHD tearing with mode numbers $m = 1$, $n \geqslant 6$ resonant at different radii in the core and $m = 0$, $n \geqslant 1$ resonant at the $q = 0$ surface near the edge of the plasma. Stochastic magnetic transport from these modes is discussed in section 4.

In standard RFP operation, $E_\phi(a)$ is held constant to maintain a stationary toroidal current, while $E_\theta(a) \approx 0$ (stationary toroidal flux except near strong dynamo events, appearing as negative E_θ spikes). Hence $E_\parallel < 0$ at the boundary of standard RFP plasmas, tending to peak and de-stabilize the current profile. To extend PPCD, $E_\phi(a)$ is instead allowed to decrease and reverse sign as shown in figure 2(*a*). Since $B_\phi(a) < 0$, reversed $E_\phi(a) < 0$ maintains $E_\parallel(a) > 0$. This is effective near the end of the toroidal field ramp when $B_\phi(a)$ is most negative. The combination of loop voltages in figure 2 produces the longest and most complete fluctuation reduction to date. A broadband and simultaneous reduction of both $m = 0$ and 1 modes generally leads to the largest confinement improvement [10, 13]. Nevertheless, PPCD programming is inherently transient, terminating in a non-disruptive loss of improved confinement conditions when the fluctuation amplitude increases.

2.1. Temperature profiles and local heat transport

The electron temperature increases dramatically when magnetic fluctuations are reduced. The $T_e(r)$ profiles for 400 kA standard and PPCD-improved plasmas are compared in figure 3(*a*), obtained with a movable, single-point Thomson scattering diagnostic at $t = 18$ ms (near the end of PPCD in figure 2). The line-averaged density is $1.0 \times 10^{19}\,\mathrm{m}^{-3}$ in both cases. The radial resolution in these profiles is the maximum acquired to date for MST, with each data point representing an average measurement for ~ 5 similar plasmas. These profiles therefore represent average PPCD-improved performance. Construction of $T_e(r)$ with less radial resolution
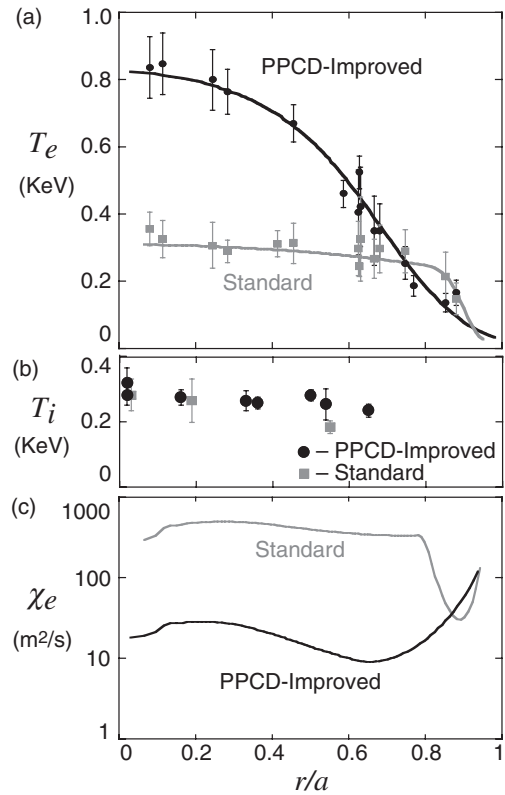

Figure 3. Radial profiles of (*a*) electron temperature, (*b*) C^{6+} ion temperature and (*c*) electron heat conductivity. Global τ_e increases five-fold in this case.

but using only the best PPCD plasmas (with longest low fluctuation periods) shows similar core temperatures but a larger T_e in the outer region of the plasma. A maximum $T_e(0) = 1.3$ keV has been measured in high quality 500 kA PPCD plasmas [13].

Reduced electron energy loss is self-evident in figure 3(*a*): the temperature increases—which decreases the Ohmic heating power—and the temperature gradient extends well into the core during PPCD. Local transport analysis confirms this result. A novel toroidal equilibrium reconstruction approach [14, 15] provides direct measurement of the local Ohmic heating power density, $\boldsymbol{E} \cdot \boldsymbol{J}$. This automatically accounts for Z_{eff}, the neoclassical (trapped electron) resistivity enhancement, and non-dissipative fast electrons, which carry <20% of the current. During PPCD, a simple Ohm's law for the parallel current is obeyed [15], and so $\boldsymbol{E} \cdot \boldsymbol{J} = \eta J^2$. The equilibrium reconstructions are constrained by 11 chords of FIR polarimetry [16], an on-axis measure of the magnetic field using the motional Stark effect [17], as well as conventional edge magnetic measurements. The electron heat conductivity profiles, $\chi_e(r)$, for standard and PPCD-improved plasmas are compared in figure 3(*c*). Losses associated with electron-ion collisions, radiation, and thermal convection are subtracted from the input power to isolate the conducted heat flux, $q_e = -\chi_e n \nabla T_e$. A dramatic decrease in χ_e is evident across the plasma radius during PPCD, and the global energy confinement time increases to $\tau_e \approx 5$ ms, a five-fold improvement relative to standard plasmas. Selecting the best PPCD plasmas, the global confinement improvement is estimated to be ten-fold to $\tau_E \approx 10 \pm 2.5$ ms, with minimum $\chi_e \sim 5\,\mathrm{m}^2\,\mathrm{s}^{-1}$ [10].

Unlike the electron temperature, the ion temperature does not change significantly, shown in figure 3(*b*) for both standard and PPCD plasmas. These profiles are the C^{6+} impurity temperature measured by charge exchange recombination spectroscopy (along a diagnostic neutral beam). The majority ion temperature profile measured by Rutherford scattering of a neutral beam is similar to the impurity ion temperature. The ions in standard plasmas are heated, in part, by a poorly understood mechanism correlated with magnetic reconnection and the dynamo producing $T_i > T_e$ at some instants in time [18]. This magnetic relaxation activity is suppressed during PPCD, but without a more quantitative understanding of the heating process, ion energy transport is difficult to quantify. The increased electron–ion temperature difference plus a reduction in charge exchange loss allows the possibility that the ions are heated by classical electron–ion collisions during PPCD. In this case the ion energy confinement time is substantially larger than the global or electron energy confinement times.

2.2. Comparison with tokamak confinement via empirical scaling

The heat conductivity, $\chi_e \sim 5\,\mathrm{m}^2\,\mathrm{s}^{-1}$, observed during PPCD is comparable with that in tokamak plasmas, and therefore the global confinement time should be comparable as well. There is no unique way to compare global confinement in different toroidal magnetic geometries, especially when a major configuration variable is substantially different, in this case the toroidal magnetic field strength. A comparison using the IPB98(y, 2) ELMy H-mode tokamak empirical scaling is shown in figure 4. The tokamak data come from the ITER physics database used to construct scaling formulae [19]. The data point labelled 'PPCD-Improved' is $\tau_E = 10\,\mathrm{ms}$ for $I_\phi = 200\,\mathrm{kA}$ PPCD plasmas plotted against the tokamak scaling-projected value $\tau_E = 23\,\mathrm{ms}$ derived from the IPB98(y, 2) engineering parameter formula calculated with
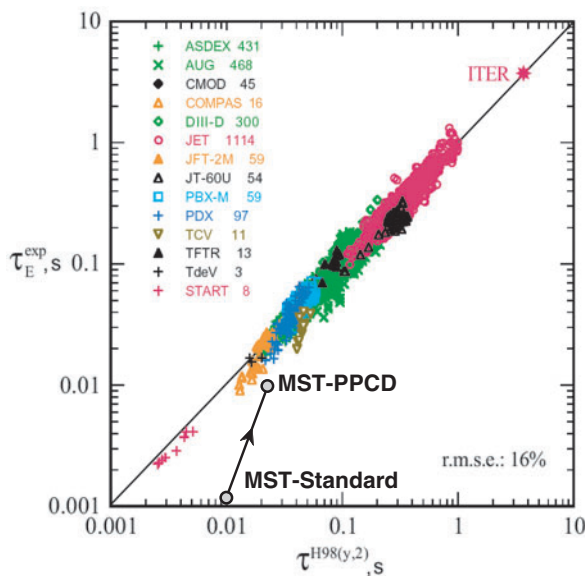

Figure 4. MST confinement relative to tokamak H-mode empirical scaling. (Reprinted from ITER Physics Guidelines, ITER report N 19 FDR 1 01-07-13 R 0.1.)

MSTs current, density $n = 0.7 \times 10^{19}\,\mathrm{m}^{-3}$, (Ohmic) input power $P = 0.5\,\mathrm{MW}$ ($\mathrm{d}W_{\mathrm{th}}/\mathrm{d}t$ subtracted), major radius, aspect ratio and circular shape ($\kappa = 1$). The point labelled 'Standard' is MSTs steady-induction confinement, $\tau_E \approx 1\,\mathrm{ms}$, compared the same way. The IPB98(y, 2) scaling's toroidal field sensitivity, $\sim B_\phi^{0.15}$, is quite weak (an interesting fact in this comparison), but $B_\phi = 1.0\,\mathrm{T}$ is chosen to represent typical tokamak operation with $q_a = 4$. For reference, the L-mode scaling-projected confinement time is $\tau_E = 18\,\mathrm{ms}$, and the neo-Alcator (Ohmic) scaling-projected confinement time is $\tau_E = 31\,\mathrm{ms}$ for the same $q_a = 4$ 'equivalent' tokamak using similar empirical formulae [19]. Note that the poloidal gyroradius is the same for tokamak and RFP plasmas if the plasma current, size and temperature are the same. Banana orbit widths are small in the poloidal-field-dominated RFP, and so the classical transport step size corresponds to the neoclassical transport step size in the same size and current tokamak.

The comparison in figure 4 shows that PPCD-improved global RFP confinement is indeed comparable with the confinement expectations for a tokamak, but with the important difference that $B_\phi(a)$ is 20 times smaller in the MST RFP than for the $q_a = 4$ 'equivalent' tokamak ($B_\phi \approx 0.05\,\mathrm{T}$ at $r = a$ for 200 kA PPCD). The total field strength at the plasma surface—including the dominant poloidal field—is ten times smaller than the equivalent tokamak. It should be emphasized that the similarity of confinement times in this comparison does not imply tokamak scaling applies to PPCD-improved RFP plasmas. Too few data exist to draw conclusions regarding the scaling of an RFP with minimized MHD tearing fluctuations, which could be very different from tokamak scalings.

2.3. Increased beta during PPCD

The increase in electron temperature during PPCD leads to a doubling of beta [10]. (Recall the line-averaged density is maintained the same.) The maximum beta is achieved in 200 kA plasmas, where the total beta, $\beta_{\mathrm{tot}} = \langle p \rangle / B^2(a)$, increases from 9% in standard plasmas to 15% during PPCD. In higher current (400 kA) plasmas the beta enhancement factor is larger, with β_{tot} increasing from 5% to 11%. Hence the beta reduction observed with increasing current in standard plasmas is substantially lessened with PPCD. Toroidal beta, $\beta_\phi = \langle p \rangle / B_\phi^2(a)$, as commonly defined for tokamak and ST experiments, is very large for the RFP since the vacuum toroidal field is small ($\beta_\phi \to \infty$ by operating with $q_a \to 0$). During PPCD, toroidal beta decreases to $\beta_\phi \approx 80\%$ since $|B_\phi(a)|$ increases as a consequence of inductive poloidal current drive. Poloidal beta $\beta_\theta = \langle p \rangle / B_\theta^2(a)$ is relatively small in the RFP since $B_\theta(a) \approx B(a)$, making it comparable with total beta.

The beta values quoted above are not identified limits, but rather the natural values that occur in these Ohmically heated plasmas. Generally beta in MST is about a factor of 2 less than the ideal MHD limit defined by interchange stability. The theoretical pressure profile that satisfies the Suydam (or Mercier) criterion at all radii defines an ideal beta limit, $\beta_\theta \approx 20\%$, for MSTs standard equilibrium, increasing to $\beta_\theta \approx 30\%$ during PPCD from increased magnetic shear. The measured pressure gradients are close to the theoretical

ideal interchange limit in the edge and core where magnetic shear is weakest, but there is no obvious phenomenon that limits the pressure. The experimental beta limiting physics in the RFP is unknown, usually speculated to be associated with resistive MHD. For example pressure-driven tearing becomes substantial at high beta values in MHD computation, and g-modes are everywhere unstable in the RFP (but with small linear growth rates when $\beta \ll 1$).

3. Confinement of fast electrons

Collisionless diffusion in a stochastic magnetic field scales as $\sim v_\parallel D_m$, where $v_\parallel$ is the parallel particle velocity and D_m is the magnetic field line diffusivity. The distribution of high energy electrons is therefore a sensitive indicator of magnetic surface quality. A $\sim$100-fold increase in hard x-ray bremsstrahlung emission during PPCD implies that the confinement of high energy electrons is vastly improved [20]. The x-ray energy flux spectra for standard and PPCD plasmas are shown in figure 5, measured using a solid state CdZnTe detector. The absence of photons with energy >20 keV in standard plasmas shows that electrons with energy above 20 keV are not confined. In contrast, electrons >100 keV are present during PPCD.

Fokker–Planck transport modelling has been used to reconstruct the x-ray flux, thereby inferring the diffusive properties of the collisionless electrons. The multi-species, toroidal, relativistic Fokker–Planck code CQL3D [21] evolves the ion and electron distributions in a Maxwellian background defined by the measured density and temperature profiles. The calculated bremsstrahlung from electron–ion collisions is compared with the measured x-ray flux, and the radial diffusion coefficient is adjusted to match the x-ray emission and, simultaneously, the measured parallel electric field and current density profiles from equilibrium reconstruction [20]. The smooth lines overlying the binned experimental data in figure 5 are the best-fit Fokker–Planck reconstructions of the x-ray flux. To achieve reasonable fits, the parallel velocity dependence in the electron diffusion coefficient for standard plasmas is $D \sim v_{\parallel e}$, characteristic of transport in a stochastic magnetic field, but for the PPCD case D is independent of the parallel velocity, suggesting stochastic loss is no longer dominant. A velocity-independent D is more characteristic of electrostatic turbulent transport like that observed in tokamak and stellarator plasmas.

4. Heat transport in a stochastic magnetic field

Although collisionless particle and energy transport in a stochastic magnetic field is fundamentally non-local, the process of field line diffusion requires local tearing and reconnection at many radii to form an extended region of magnetic stochasticity. The safety factor profile, $q(r)$, for typical standard plasma conditions in MST is shown in figure 6(*a*), determined by toroidal equilibrium reconstruction. The large magnetic shear associated with $q \to 0$ permits many low-mode-number rational surfaces on which magnetic islands can form. The close spacing of these surfaces renders the magnetic field susceptible to island overlap, especially near $q = 0$. The dominant magnetic fluctuations observed in the RFP are $m = 1$, $n > q(0)^{-1} \approx 5$ tearing modes resonant inside the reversal surface, as well as $m = 0$ modes resonant at the $q = 0$ surface. The typical magnetic island widths associated with the $m = 1$, $n \leqslant 15$ modes are superposed on the $q(r)$ profile in figure 6(*a*). A toroidal array of 32 magnetic sensors measures the amplitudes of these modes at the plasma surface in MST. Since the islands overlap, it is not surprising that stochastic diffusion would dominate standard RFP transport.
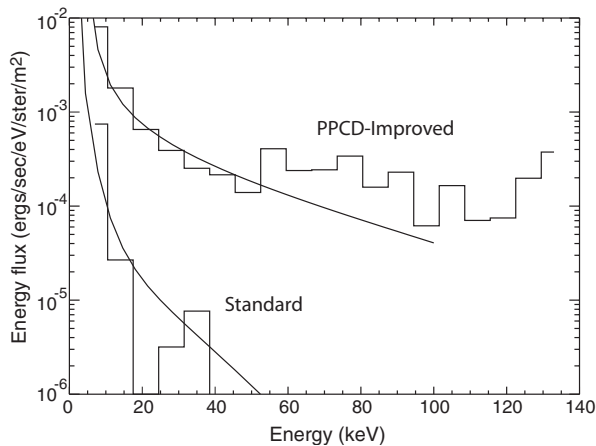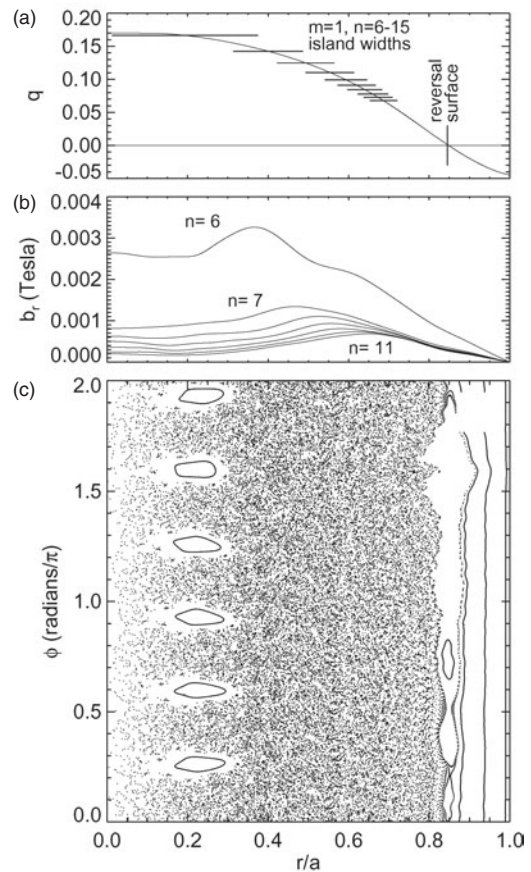

Figure 5. Hard x-ray energy flux spectra for standard and PPCD plasmas. The jagged curves are binned x-ray measurements, and the smooth curves are fits from Fokker–Plank modelling.

Figure 6. (*a*) Standard RFP $q(r)$ with $m = 1$ island widths, (*b*) profiles of core-resonant $m = 1$ radial magnetic fluctuations and (*c*) field line tracing puncture plot in axial (toroidal) plane.

4.1. Comparison with theoretical expectations for electron heat transport

Recent improvements in magnetic and kinetic profile diagnostics in MST permit a more quantitative comparison of the measured transport coefficients with theoretical expectations for stochastic diffusion. Furthermore the PPCD-controlled reduction of magnetic fluctuations permits investigation of the dependence on the magnitude and structure of the magnetic fluctuations. The diffusion of high energy electrons in standard RFP plasmas was reported in section 3 to have the expected parallel velocity dependence. The heat conduction for bulk electrons in standard plasmas is also well described by stochastic transport expectations, provided the magnetic diffusivity is determined more directly than the often-used correlation length estimates.

Magnetic field line tracing is used to quantify the magnetic diffusivity resulting from the dominant fluctuations in MST standard plasmas [22]. The mean-field profiles are taken from an experimental equilibrium reconstruction, while the fluctuating-field profiles are taken from three-dimensional (cylindrical), non-linear, resistive MHD computation using the DEBS code [23] (in lieu of directly measured fluctuation profiles, which are not yet available). Such computation has long been used for theoretical investigation of the MHD dynamo process that occurs in standard RFP plasmas, reproducing experimental fluctuation characteristics and dynamo behaviour remarkably well. To model MST plasmas, the MHD computation is performed at an effective aspect ratio of $R/a = 3$ and Lundquist number of $S \approx 10^6$, very close to the experimental value $S \approx 3 \times 10^6$ for the $\sim$400 kA case described here. The resistivity profile measured in MST is also used.

The profiles of the computed radial magnetic fluctuations, $\tilde{b}_{rn}(r)$, are shown in figure 6(b) for the dominant $m = 1$ modes. The field line puncture plot shown in figure 6(c) illustrates the widespread magnetic stochasticity expected from these modes in the core of standard RFP plasmas. Island structure is evident only for the innermost mode $m = 1$, $n = 6$ and for $m = 0$ modes at the reversal surface. To best simulate the experiment, the mode amplitudes are normalized to match the transverse field fluctuation at the plasma surface, even though the computation predicts the measured amplitudes to within 20%. To model possible stochasticity out to the reversal surface, $m = 1$ modes with $n \leqslant 32$ are included in the field line tracing code. The amplitudes of modes $16 \geqslant n \geqslant 32$ are extrapolated from the measured spectrum, $n \leqslant 15$. Note that the radial mode structure is global in extent. A thick conducting shell surrounds MST plasmas, thus forcing $b_r(a) = 0$. (Perfect-conductor boundary conditions are used in the computation at $r = a$.) The non-stochastic boundary outside the reversal surface results from $b_r \to 0$ as $r \to a$.

The magnetic diffusivity is calculated directly from field line tracing by forming the ensemble average $D_m = \langle \Delta r^2 / \Delta L \rangle$ for the field line radial excursion, Δr, over the field line length, ΔL. The predicted heat conductivity for stochastic magnetic transport $\chi_e = v_{T_e} D_m$ is compared with the measured (power balance) χ_e in figure 7(a), agreeing surprisingly well. The field line tracing reproduces large $\chi_e \sim 500 \, \text{m}^2 \, \text{s}^{-1}$ in the core, as well as the relative transport barrier $\chi_e \sim 50 \, \text{m}^2 \, \text{s}^{-1}$ near the $q = 0$ reversal surface. Although the line tracing may
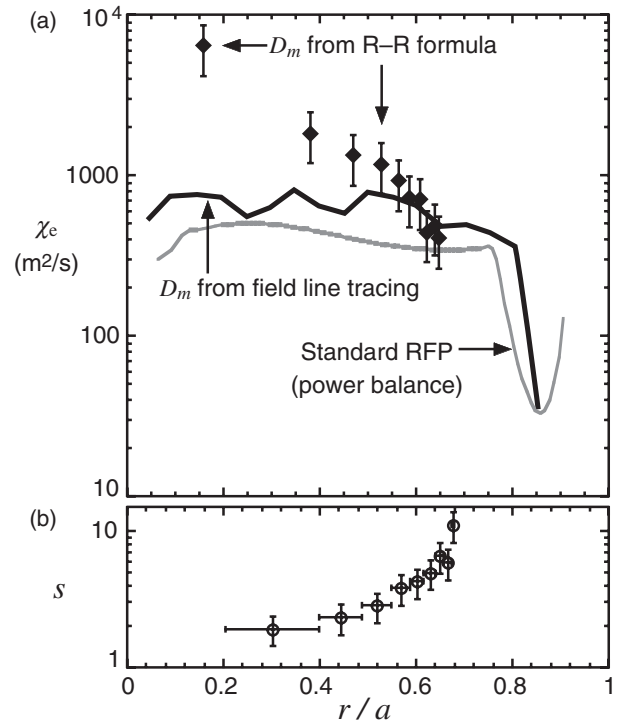

Figure 7. (a) Calculated stochastic–magnetic heat conductivity $\chi_e = v_{T_e} D_m$ compared to measured χ_e in standard plasmas and (b) Chirikov island overlap parameter versus radius.

not be fully accurate near the reversal surface, $\chi_e \sim 50 \, \text{m}^2 \, \text{s}^{-1}$ is consistent with the measured global energy confinement time of $\tau_E \approx 1$ ms. The $q = 0$ surface is unique because all $m = 0$ modes are resonant at the same location and because the magnitude of $\tilde{b}_{rn}$ is relatively small compared with $m = 1$ modes, both from the close proximity to the conducting shell at $r = a$ and from the longer wavelength of $m = 0, n \sim 1$ modes. The magnetic transport associated with $m = 0$ modes should be smaller as a result. More $m = 1$ modes need to be included in the field line tracing to resolve the region surrounding the reversal surface.

The often-used estimate $\chi_e^{\text{RR}} = v_{T_e} \pi L_{\text{eff}} \tilde{b}_{rn}^2 / B^2$ derived by Rechester–Rosenbluth [24] is also shown in figure 7(a) using the single-mode amplitudes for $n \leqslant 15$. In contrast to direct field line tracing, the R–R estimate agrees with the measured χ_e only in the region where the resonant surface density is highest, just inside the reversal surface. The Chirikov parameter, $s = (w_{mn} + w_{m'n'})/2(r_{mn} - r_{m'n'})$, which measures the overlap of adjacent islands of width w_{mn} located at resonant surfaces r_{mn}, is shown in figure 7(b). An accurate estimate using the Rechester–Rosenbluth formulation appears to require $s > 5$. Note that although the mode amplitudes are largest in the core, the islands are weakly overlapped there ($s \sim 1$), yielding a much a smaller heat conductivity value than estimated by χ_e^{RR}.

4.2. Role of the mode spectrum for improved RFP confinement

The localized nature of resonant field line tearing is well illustrated in the standard RFP. Many adjacent resonant modes

of significant amplitude are required to diffuse field lines across the radius of the plasma. Note in figure 3(*c*) that χ_e during PPCD is greatly reduced where the magnetic stochasticity is most intense in standard RFP plasmas, just inside the $q = 0$ surface (see figures 6 and 7). The broad spectrum of higher-n, $m = 1$ modes resonant at mid-radius must therefore be strongly influenced by PPCD. The fluctuation reduction shown in figure 2(*c*) is the total spectral rms, dominated by the largest mode, $m = 1$, $n = 6$, resonant near the magnetic axis. The reduction in the higher-n modes resonant at mid-radius is typically greater.

The maximum $T_e(0)$ achieved during PPCD—a good single-indicator of energy confinement in an Ohmically heated plasma—occurs when the time-average amplitudes of the mid-radius modes are smallest. This is shown in figure 8(*a*), where $T_e(0)$ near the end of PPCD ($t = 18$ ms in figure 2) is plotted against the rms fluctuation amplitude, $\sqrt{\sum_n b_{\theta n}^2}(a)$, summed for $8 \leqslant n \leqslant 15$ and time-averaged from the start to end of PPCD ($t = 12$–18 ms in figure 2). The data points labelled '+' are measurements from individual plasmas with the same current and density formed with identical PPCD programming. The data point labelled 'Standard' is plotted for the $T_e(0)$ and high-n rms mode amplitude in standard plasmas with the same current and density. To maximize the number of shots available for this analysis, a double-filter (Be) soft x-ray measurement of the core electron temperature is used, calibrated to Thomson scattering measurements of the core temperature, $T_e(r/a < 0.2)$, obtained in a subset of the shots.

The variation in degree of fluctuation reduction for individual plasmas reveals a clear correlation of higher $T_e(0)$ with sustained low amplitudes of the mid-radius resonant modes during PPCD. Note, however, that the ~30-fold reduction of the mid-radius, χ_e, is significantly larger than a typical ~7-fold reduction of b_{rms}^2 for the mid-radius resonant modes. So although the trend in figure 8(*a*) suggests that

magnetic fluctuations still regulate transport during PPCD, the reduction in χ_e is larger than expected from the b^2-scaling characteristic of stochastic transport. The $v_\parallel$-independent diffusion of fast electrons discussed in section 3 is clearer evidence for a non-stochastic residual transport mechanism, which might still have an electromagnetic origin but with a different $\tilde{B}$-dependence.

The importance of broadband mode suppression for improved confinement is further revealed in a similar plot of $T_e(0)$ and magnetic fluctuation amplitude shown in figure 8(*b*), but for the dominant $m = 1$, $n = 6$ mode resonant close to the magnetic axis in the same plasmas. The $n = 6$ is the largest mode in the spectrum in the vast majority of MST plasmas, sometimes increasing in magnitude during PPCD. (The adjacent $n = 7$ mode is rarely larger.) Two striking features are revealed in figure 8(*b*). First, the correlation between $T_e(0)$ and the dominant—and therefore total—fluctuation amplitude is weak. Second, the temperature in the core is weakly influenced by the nearest resonant mode. Both features are understandable considering the discussion above for magnetic transport in RFP plasmas. The core temperature is being supported by low heat conductivity in the mid-radius region where many high-n modes are resonant. A large mode resonant in the core weakly impacts global confinement. Transport within an isolated island may be large, but not beyond its outer radius. This is analogous to the weak impact of $m = 1$, $n = 1$ sawtoothing on tokamak plasma confinement when the $q = 1$ surface remains close to the magnetic axis. Note that some PPCD plasmas in figure 8 have simultaneously one relatively large core-resonant mode and a broad spectrum of small higher-n modes.

5. Other plasma control tools

Transient inductive current drive has become a very effective tool for magnetic fluctuation and transport control in the RFP. Although PPCD-like inductive current drive could be attractive in a pulsed-reactor scenario (e.g. self-similar current ramp-down [25]), non-transient rf techniques have potential for more precise and localized profile control to extend and refine current profile control. Lower-hybrid (LH) and electron Bernstein wave (EBW) scenarios are being tested at low power in MST. Ac helicity injection, sometimes called OFCD, is being tested for steady-state inductive current sustainment and possibly profile control. In addition to current drive, either rf scenario would provide auxiliary heating as well. The more direct approach using neutral beam injection is also being evaluated. No substantial auxiliary heating has been used in RFP research to date, partly because Ohmic heating has always been large. Since beta and confinement are coupled in Ohmically heated plasma, auxiliary heating would permit direct investigation of the unknown beta-limiting phenomena in the RFP.

Ray-tracing calculations have shown the LH wave to be a good candidate for current profile control in the RFP [26]. A second-generation interdigital-line, travelling wave antenna is installed in MST for launching 800 MHz, $n_\parallel \sim 8$ LH waves. The achieved input power is ~40 kW with low ~10% reflection, nearly the maximum available from the installed 50 kW power supply. Probe instrumentation measures an e-folding length, ~20 cm, of the damped power along the
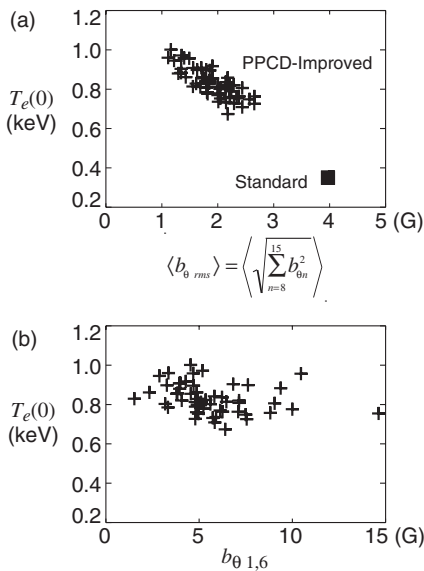

Figure 8. (*a*) Core electron temperature versus time-average rms fluctuation amplitude of $8 \leqslant n \leqslant 15$ modes. (*b*) Core electron temperature versus amplitude of the dominant mode $m = 1$, $n = 6$. These data are for 400 kA plasmas with line-averaged density 1.0×10^{19} m^{-3}.

antenna from plasma loading, roughly four rf wavelengths, $\lambda_{LH} = 4.8$ cm. This damping length allows a launched wavenumber spectrum appropriate for current drive. A small feedthrough port size is one of the attractive features of the interdigital-line approach, well suited to MST. Multiple antennas are anticipated to achieve the ~1–2 MW requirement for current profile control experiments.

The observation of thermal levels of electron cyclotron emission suggests, by reciprocity, that EBW current drive and heating can be done in the overdense RFP [27]. A twin waveguide antenna has been installed on a 11.4 cm port to launch 3.1–3.8 GHz waves in MST from two travelling-wave tubes providing ⩽120 kW total power. At low power, the amplitude of the reflected power varies with the relative phasing of the two waveguides, in qualitative agreement with theoretical analysis of coupling. Moreover the coupling is best during PPCD, bolstering the viability of EBW current profile control. The available 120 kW is ~5–10% of the Ohmic heating power during PPCD, and so rf heating might be an observable perturbation in temperature-related measurements. A search for absorption signatures in soft and hard x-ray emission is presently underway.

Current sustainment in the RFP is especially difficult, given that the pressure-driven neoclassical bootstrap current is small. A long-standing hope for the RFP is ac helicity injection using low frequency sinusoidal modulation of the inductive loop voltages, sometimes called OFCD. Bevir and Gray [28] recognized that $\pi/2$ relative phasing of the loop voltages injects time-average dc magnetic helicity to maintain a dc plasma current (with small ac modulation) if the plasma maintains a relaxed state. Two ~500 Hz, <1 MVA oscillators have been installed in MSTs Ohmic circuits to test partial current drive by OFCD. First results are shown in figure 9. The additional current provided by low power OFCD is small (as expected). The dependence on the relative phase of the oscillators agrees very well with helicity injection expectations, reproducing a key result from the first (and only other) OFCD experiment in ZT-40M [29]. New three-dimensional, non-linear, resistive MHD computation at high Lundquist numbers demonstrates sustainment of dc plasma current with sinusoidal loop voltages, forming a theoretical basis to evaluate and optimize OFCD experiments in MST [30]. A key issue to be explored is compatibility with confinement, since OFCD is based on the relaxation physics that operates in standard RFP plasmas.

A low current (diagnostic) neutral beam [31] has been used for the first exploration of fast ion confinement in the RFP. Figure 10 shows measured fast charge-exchange neutrals observed following the abrupt shut-off of the neutral beam in standard RFP plasmas. In the two cases shown, 1 A equivalent H neutrals were injected at 10 and 20 kV perpendicular to the plasma along a central chord. The slow decay of the fast ion background greatly exceeds not only the bulk particle confinement time, ~1 ms, but also the loss time expected for stochastic-magnetic diffusion, $\sim v_{\parallel} D_m$, with D_m inferred from χ_e measurements in the core (figure 7). The loss rate is identical for both 10 and 20 kV injected neutrals, also uncharacteristic of stochastic diffusion. Finite gyroradius averaging could explain why fast ions are more weakly affected by magnetic stochasticity than fast electrons in standard RFP plasmas. Preliminary particle orbit modelling for the stochastic field
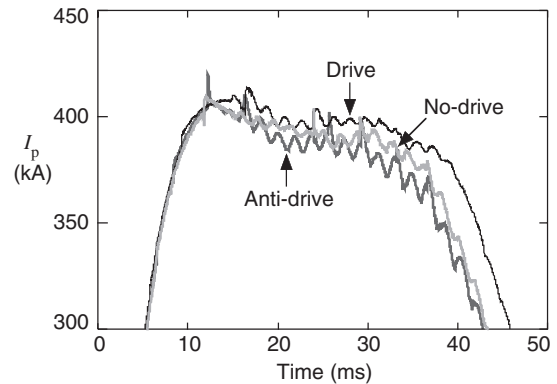

Figure 9. Toroidal plasma current with OFCD oscillators phased for current drive ('Drive', top waveform), no current drive ('No-drive', middle waveform) and anti-current drive ('Anti-drive', bottom waveform). The toroidal current with the oscillators turned off closely follows the 'No-drive' waveform.
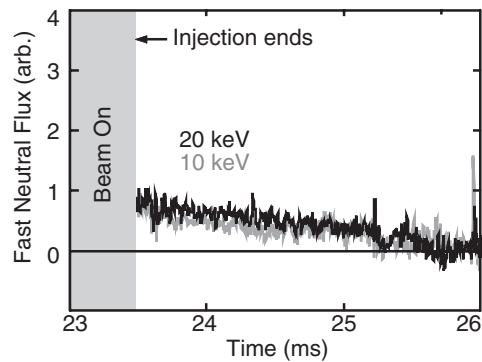

Figure 10. Decay of fast neutral background following abrupt neutral beam turn-off.

described in section 4.1 and shown in figure 6 indicates that the particle diffusion is reduced ~4-fold for a 10 keV proton ($\rho_i/a \approx 0.08$), relative to the zero-gyroradius Rechester–Rosenbluth expectation. This proton's gyroradius is larger than both the typical island width and the spacing between resonant surfaces in the middle of the plasma. A short pulse ~1 MW beam is being tested as the next step towards high power neutral beam heating. Fast-ion confinement will be examined in greater detail for tangential beam injection.

6. Summary

Energy confinement comparable with tokamak quality has been obtained in the MST RFP at a high beta and low toroidal magnetic field. Magnetic fluctuations, which cause widespread magnetic stochasticity in the core of standard RFP plasmas, are reduced by inductive current drive targeted to the edge region of the plasma. Fast electrons >100 keV are confined, and Fokker–Planck modelling infers that the diffusion of these high energy electrons is independent of their parallel velocity, therefore not due to stochastic magnetic transport. The nature of the residual transport, whether electromagnetic or electrostatic as observed for turbulent transport in tokamak and stellarator plasmas, is an interesting open question. In contrast, the heat diffusivity in standard plasmas agrees well with stochastic transport expectations.

The global energy confinement improves ten-fold to a value comparable with an equivalent tokamak of the same current, density, heating power, size and shape, but with 20 times smaller applied toroidal field in the MST RFP. A strong correlation between high core temperature and low $m = 1$, $n \geqslant 8$ mode amplitudes reveals the importance of sustained reduction of resonant modes in the mid-radius region inside the $q = 0$ surface.

The inductive techniques used to create improved confinement in MST are inherently transient (but relevant to plausible pulsed reactor scenarios). To sustain and refine current profile control, rf current drive is in development. LH and EBW injection experiments are under way at low power. If successful, the rf techniques could provide auxiliary heating as well as localized current drive. Good fast-ion confinement revealed through diagnostic neutral beam injection suggests efficient neutral beam heating might be possible as well. High power, short pulse beam injection experiments are beginning. Lastly, current sustainment by ac helicity injection (or OFCD) is being tested. Fractional current drive in accordance with helicity balance predictions is observed with low power oscillators.

Acknowledgment

References

[1] Najmabadi F. *et al* 1990 The TITAN reversed field pinch reactor study—the final report *UCLA Report* UCLA-PPG-1200

[2] Stoneking M.R. *et al* 1998 *Phys. Plasmas* **5** 1004
[3] Capello S. and Biskamp D. 1996 *Nucl. Fusion* **36** 571
[4] Capello S. and Paccagnella R. 1992 *Phys. Fluids* B **4** 611
[5] Finn J. *et al* 1992 *Phys. Fluids* B **4** 1262
[6] Martin P. *et al* 2003 *Nucl. Fusion* **43** 1855
[7] Sovinec C.R. and Prager S.C. 1999 *Nucl. Fusion* **39** 777
[8] Sarff J.S. *et al* 1994 *Phys. Rev. Lett.* **72** 3670
[9] Bartiromo R. *et al* 1999 *Phys. Rev. Lett.* **82** 1492
[10] Chapman B.E. *et al* 2001 *Phys. Rev. Lett.* **87** 205001
[11] Yagi Y. *et al* 2003 *Phys. Plasmas* **10** 2925
[12] Dexter R.N. *et al* 1991 *Fusion Technol.* **19** 131
[13] Chapman B.E. *et al* 2002 *Phys. Plasmas* **9** 2061
[14] Anderson J.K. *et al* Equilibrium reconstruction in the Madison Symmetric Torus reversed field pinch *Nucl. Fusion* submitted
[15] Anderson J.K. *et al* 2003 Dynamo-free plasma in the reversed field pinch *Phys. Rev. Lett.* submitted
[16] Brower D.L. *et al* 2002 *Phys. Rev. Lett.* **88** 185005
[17] Craig D.J. *et al* 2001 *Rev. Sci. Instrum.* **72** 1008
[18] Den Hartog D.J. *et al* 2000 *Plasma Phys. Control. Fusion* **42** L47
[19] ITER Physics Expert Groups on Confinement and Transport and Confinement Modeling and Database 1999 *Nucl. Fusion* **39** 2175
[20] O'Connell R. *et al* 2003 *Phys. Rev. Lett.* **91** 045002
[21] Harvey R.A. 1992 *GA report* GA-A20978
[22] Biewer T.M. *et al* 2003 *Phys. Rev. Lett.* **91** 045004
[23] Schnack D.D. *et al* 1987 *J. Comput. Phys.* **70** 330
[24] Rechester A. and Rosenbluth M. 1978 *Phys. Rev. Lett.* **40** 38
[25] Nebel R.A., Schnack D.D. and Gianakon T.A. 2002 *Phys. Plasmas* **9** 4968
[26] Uchimoto *et al* 1994 *Phys. Plasmas* **1** 3517
[27] Forest C.B. *et al* 2000 *Phys. Plasmas* **7** 1352
[28] Bevir M.K. *et al* 1985 *Phys. Fluids* **28** 1826
[29] Schoenberg K.F. *et al* 1984 *Phys. Fluids* **27** 2881
[30] Ebrahimi F. *et al* 2003 *Phys. Plasmas* **10** 999
[31] Abdrashitov G.F. *et al* 2001 *Rev. Sci. Instrum.* **72** 594